Scale effects on a single-element inverted wing in ground effect

J. Correia
j.correia@cranfield.ac.uk
L. S. Roberts, M. V. Finnis and K. Knowles
Aeromechanical Systems Group
Cranfield University
Shrivenham, UK

ABSTRACT

A study was conducted on a GA(W)-1 wing in order to investigate the effect of testing inverted wings in ground effect at low Reynolds numbers. The wing was tested at a range of ground clearances and Reynolds numbers and results showed that the wing's performance was dependent on both these parameters. Surface flow-visualisation and numerical simulation results highlighted the existence of a laminar separation bubble on the wing's suction surface. The results also indicated that both the bubble's length and the onset of separation were sensitive to ground clearance and Reynolds number. Attempts were made to minimise the wing's Reynolds number dependency by using transition strips on the suction surface. The transition strip results highlighted the influence that a laminar separation bubble has on the overall performance of the wing and how its presence alters the force enhancement and reduction mechanisms on an inverted wing in ground effect.

Paper No. 3993. Manuscript received 24 April 2013, revised version received 28 February 2014, accepted 6 March 2014.

https://doi.org/10.1017/S0001924000009544 Published online by Cambridge University Press

NOMENCLATURE

c	wing chord
C_D	drag coefficient, $D/q_\infty S$
C_F	downforce coefficient, F/q_∞S
C_{Fmax}	maximum downforce coefficient
C_P	pressure coefficient, $\Delta P/q_\infty$
C_{SF}	skin friction coefficient
D	drag
F	downforce
h	ground clearance
L_b	separation bubble length
P	static pressure
q_∞	freestream dynamic pressure
Re	Reynolds number, $U_\infty c/v$
S	wing planform area
U_∞	freestream velocity
x,y	cartesian co-ordinates: x – downstream, y – vertically up
x_r	separation bubble reattachment point
x_s	separation bubble onset of separation
α	angle-of-attack
v	air kinematic viscosity

1.0 INTRODUCTION

The use of scaled wind-tunnel models can lead to differences in the force coefficients between the models in the wind tunnel and the full-scale component. These scaling effects are typically due to differences in the boundary-layer transition location between the model and the full-size component at different Reynolds numbers[1]. To avoid this, boundary-layer trips are used to fix the transition point of the scaled model to the same point that would feature on the full-scale component. General guidelines for boundary-layer transition fixing using grit are presented by Braslow and Knox[2]. In their report the procedure for calculating the grit size required for fixing transition is presented, but no information on pattern, density and streamwise length of the transition strip is given.

When testing a wing at low Reynolds numbers the presence of a laminar separation bubble may be expected[3]. Liebeck and Blackwelder[4] described the formation of such a phenomenon as follows.

1. An adverse pressure gradient causes separation of the laminar boundary layer.
2. Growth of inviscid instabilities, such as Kelvin-Helmholtz type, causing disturbances in the separated shear layer which lead to turbulence production.
3. As turbulence grows increased mixing and the entrainment of higher velocity flow causes reattachment to the wall as a turbulent boundary layer.

Therefore, the presence of a separation bubble shows that the transition mechanism differs from the natural transition case that would be expected on a flat plate.

Studies of the behaviour of such laminar separations have shown that the length of the separation bubble decreases with increasing Reynolds number[5], the onset of separation is dependent on Reynolds number[6], and that as the Reynolds number increases the height of the bubble decreases at a greater rate than its length[7]. However, no study appears to have been made of the behaviour of the laminar separation bubble in ground effect.

https://doi.org/10.1017/S0001924000009544 Published online by Cambridge University Press

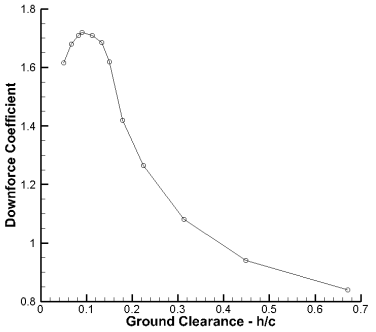


Figure 1. Typical behaviour of an inverted wing in ground effect[8] (Tyrrell 026 wing section, $\alpha = 1°$, Re = 4·47 ×

Most monoposto, open-wheel racing cars generate downforce by the use of inverted wings in ground effect. Often the cars are developed in wind tunnels using scaled models at Reynolds numbers significantly lower than those experienced at full scale, typically at half to a quarter of the full-size component on a track, although full-scale Reynolds numbers can still be low enough that laminar separation can be expected.

Zerihan and Zhang[8] showed that an inverted wing in ground effect will experience an increase in downforce as its ground clearance is reduced (Fig. 1). This is known as the force-enhancement region. This increase with reducing ground clearance occurs until a critical ground clearance is reached, after which further ground clearance reductions lead to a decrease in downforce; known as the force-reduction region. Transition between the force-enhancement and -reduction regions was shown to occur when the ground clearance was reduced such that the boundary layer separated from the suction surface at the trailing edge. As the ground clearance is further reduced the separated region gradually moves forward, until the boundary layer separates completely from the wing's suction surface and the wing enters the force-reduction region.

Although the performance of inverted wings in ground effect is well documented[8-17], only a limited number of studies have reported scaling effects on inverted wings in ground effect[8,13]. Despite scale effects being well documented in the aeronautical sector, no study has yet been published that attempts to understand it or the techniques to minimise or eliminate it for ground-effect cases.

The present work aims to investigate scale effects and to show how ground proximity affects the boundary-layer behaviour on an inverted wing in ground effect. An investigation of different transition-fixing configurations is presented in an attempt to reduce the scale effect when testing at low Reynolds numbers in a wind tunnel.

2.0 EXPERIMENTAL DETAILS

2.1 Test facility

The experiments were conducted in Cranfield University's DS Houghton wind tunnel at the Defence Academy of the UK, Shrivenham. This is a 2·7m × 1·7m closed-return, three-quarter-open test section wind tunnel with freestream turbulence level of 0·7%. It is equipped with a continuous-belt rolling road synchronised with the freestream velocity, which was used to model correctly the wing moving over a stationary road. Upstream of the rolling road, boundary-layer suction was applied through perforated plates to remove the wind-tunnel boundary layer. Optimisation of the level and

https://doi.org/10.1017/S0001924000009544 Published online by Cambridge University Press

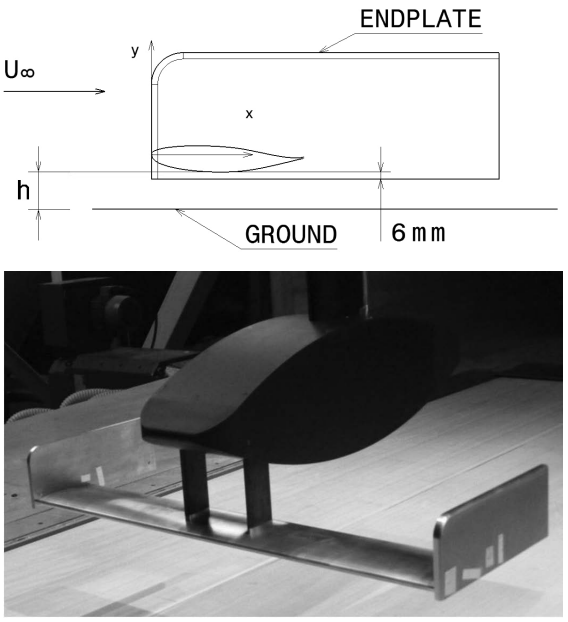


Figure 2. Wind-tunnel model: (a) wing profile and co-ordinate system; (b) assembly.

distribution of the suction, coupled with a knife-edge transition to the belt, gave a boundary layer of 1·58mm thickness at the leading edge of the wing. The wind tunnel was equipped with an overhead support sting incorporating an automated motion control system used to adjust the model's ground clearance above the rolling road during the experiments. Further information on this tunnel is given by Knowles and Finnis[18].

2.2 Model

The tests were conducted on an untapered, untwisted, rectangular-planform, GA(W)-1 section single-element wing, which has been studied previously by Knowles *et al*[9]. The present tests were completed at an incidence of –0·5° with endplates fitted from a double-element wing configuration (Fig. 2(a)). The wing had a span of 750mm and a chord of 119·7mm, corresponding to an aspect ratio of approximately 6·27. The wing was suspended by two fixed vertical struts (similar to those supporting a racing car's front wing) to a six-component Aerotech force balance positioned inside a non-metric streamlined body (Fig. 2(b)). This streamlined body isolated the force balance from the airflow and simulated the nose cone of a Formula-type racing car.

2.3 Experimental procedure

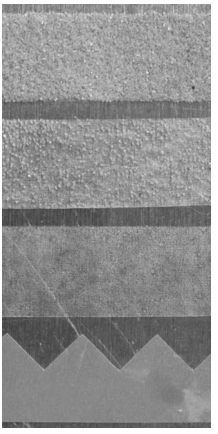
Forces were measured out of ground effect and over a range of ground clearances in ground effect, and at a range of freestream velocities from 17·5ms^{-1} to 35ms^{-1}, corresponding to chord Reynolds numbers of 1·42 $\times 10^5$ to 2·85 $\times 10^5$. The Reynolds number was assessed to be accurate to ±470. The ground clearance was defined by the distance between the lowest point on the wing surface and the ground (see Fig. 2(a)).

The force data were acquired at a frequency of 10Hz for 20 seconds at each ground clearance during the experiments using the Pi Mistral system which controlled wind-tunnel operation and data acquisition. Before and after each run nil-force data were acquired to account for any offsets

https://doi.org/10.1017/S0001924000009544 Published online by Cambridge University Press

Table 1
Transition strip description

T1	Grit applied to double-sided tape covering entire tape surface. Trip height: 0.415mm Grit distribution: 0·330g/cm^2
T2	Grit applied to double-sided tape in random pattern. Trip height: 0·415mm Grit distribution: 0·068g/cm^2
T3	Double-sided tape without grit Trip height: 0·150mm
T4	Vinyl strip with serrated leading edge. Trip height: 0·250mm



in the measurements during the experiment. The uncertainty for measured drag and lift coefficients was $2{\cdot}3 \times 10^{-3}$ and $1{\cdot}4 \times 10^{-2}$ respectively at a 95% confidence level, which was calculated based on the variables affecting the experiments i.e. pitch, roll, yaw, dynamic pressure, ground clearance, and force balance error.

Fixed-transition tests were also conducted using transition strips 12mm long ($0{\cdot}100c$) in the streamwise direction applied to the suction surface of the wing. Tests were conducted with the transition strips positioned with their leading edge at different chord-wise positions ($0{\cdot}1c$, $0{\cdot}2c$ and $0{\cdot}25c$) and at selected Reynolds numbers. Using the procedure proposed by Braslow and Knox[2] a grit size of 265μm (grit 60) and position of $0{\cdot}1c$ was calculated for $U_\infty = 25$mm, as the requirement to cause transition. In addition it was verified that the grit size satisfied the von Doenhoff and Horton[19] criterion for roughness Reynolds number for transition. The four different transition strip configurations are shown in Table 1.

Surface flow visualisation tests, using a mixture of fluorescent pigment and paraffin, were also conducted at a selection of ground clearance, Reynolds number and transition strip configurations.

2.4 Numerical simulation

As the wind-tunnel model did not include static pressure measurements, numerical simulation in MSES was employed to determine surface pressure distribution. MSES is a two-dimensional flow solver developed by Prof. Mark Drela at the Massachusetts Institute of Technology, which allows for the design and analysis of multi-element aerofoils. It is based on the solution of the inviscid Euler equations coupled with a two-equation integral formulation to describe the boundary layer and wake using a finite volume discretisation. The inviscid and viscous regions are coupled through the boundary-layer displacement thickness for which each sets the boundary condition for the other. The resulting system of nonlinear equations is then solved using the Newton method.

Laminar-turbulent transition of the boundary layer is computed through a simplified variant of the e^N method[20] known as the 'envelope method' which determines the amplitude of the most amplified Tollmien-Schlichting wave frequency at each surface point. The transition point can be controlled by the critical amplification factor N. Smith and Gamberoni[21] completed several experiments to correlate the transition point with the real part of the Orr-Sommerfeld eigenvalue and found that when disturbances had grown by approximately 8,000 times (e^9) the point of natural stability transition would occur; although van Ingen suggested lower values of e^7 or e^8 be used. Comparison of surface flow-visualisation and numerical results for the formation of the separation bubble led to a criterion of e^7 being used in the present work.

https://doi.org/10.1017/S0001924000009544 Published online by Cambridge University Press

Simulations were completed using a non-dimensionalised GA(W)-1 aerofoil section at –0·5° incidence at defined Reynolds numbers with the ground plane represented through use of the mirror-image technique.

3.0 EXPERIMENTAL RESULTS

3.1 Force measurements

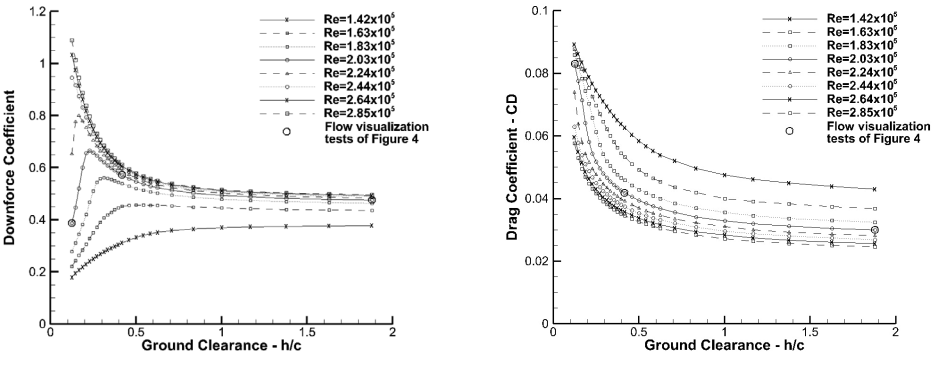
The downforce coefficient (C_F) results at different ground clearances and Reynolds numbers are shown in Fig. 3(a). The figure shows C_F increasing as Reynolds number is increased. Also apparent is the reduction of the ground clearance for C_{Fmax} as the Reynolds number is increased and a change of the stall (force reduction) characteristics, with stall becoming more abrupt as the Reynolds number is increased.

The results for Reynolds numbers between $1{\cdot}63 \times 10^5$ and $2{\cdot}03 \times 10^5$ show C_F increasing as ground clearance is reduced until reaching the ground clearance of C_{Fmax}. Below this, further reductions in ground clearance lead to a reduction in C_F. For $Re < 1{\cdot}63 \times 10^5$ the results show a reduction of C_F with reducing ground clearance throughout the ground clearance range without reaching the force enhancement region, while for $Re \geq 2{\cdot}44 \times 10^5$ C_F gradually increases throughout the ground clearance range without reaching C_{Fmax} and entering the force reduction region. It is anticipated that at lower ground clearances than those tested here, these high-Reynolds number cases will also experience force reduction (as seen in the data of Fig. (1)).

The drag coefficient (C_D) results are shown in Fig. 3(b), which shows C_D increasing in all cases as ground clearance is decreased. The figure also shows C_D decreasing as Reynolds number is increased. Clearly, Fig. 3 shows a Reynolds number dependency of the measured forces. Possible reasons for this will now be investigated by means of surface flow-visualisation and numerical simulation, before tripping of the boundary layer is explored.

3.2 Flow visualisation

Surface flow visualisation was carried out on the wing's suction surface at a number of ground clearances and Reynolds numbers. The 'paint' was sprayed onto the wing, which was then run in the tunnel for 45 minutes in order to let the flow pattern dry. The wing was then removed from the tunnel and photographs taken under ultra-violet light.



(a) (b)

Figure 3. (a) Downforce coefficient, C_F and (b) drag coefficient, C_D at different Reynolds numbers untripped wing.

https://doi.org/10.1017/S0001924000009544 Published online by Cambridge University Press

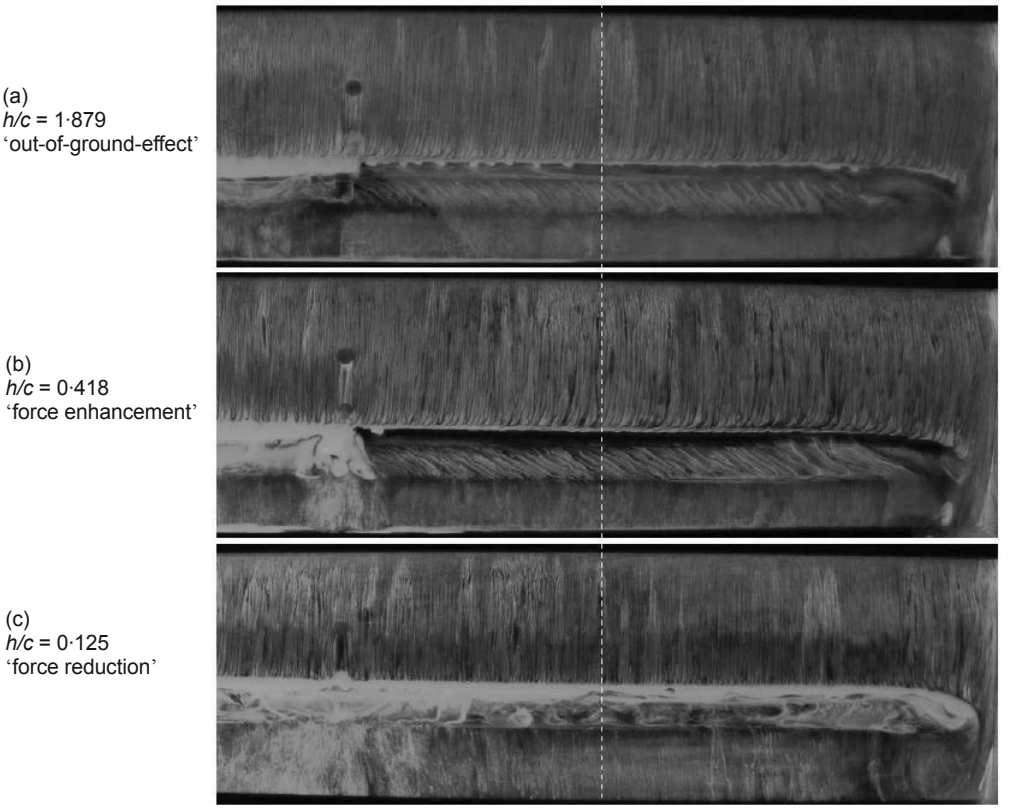


Figure 4. Semi-span flow visualisation results at different *h* and at Re = 2·03 x 10^5. (leading edge uppermost, wing tip on the right).

The results for Re = 2·03 ×10^5 at three different ground clearances are shown in Fig. 4. The three different ground clearances shown in Fig. 4 represent the out-of-ground-effect condition, the force enhancement and force reduction regions, as indicated in Fig. 3.

Table 2
Variation with Reynolds number of separation (x_s) and reattachment (x_r) locations, and bubble length (L_b)

Re (U_∞)	2·03 × 10^5 (25ms^{-1})			2·85 × 10^5 (35ms^{-1})		
h/c	x_s/c	x_r/c	L_b/c	x_s/c	x_r/c	L_b/c
1·879	0·60	0·80	0·20	0·60	0·79	0·19
0·418	0·58	0·78	0·20	0·60	0·78	0·18
0·125	0·53	0·71	0·18	0·56	0·70	0·14

The figure shows the presence of a laminar separation bubble on the wing's surface at all ground clearances. Analysis of the bubble separation (x_s), reattachment (x_r) and length (L_b), for Re 2·03 ×10^5 and Re = 2·85 ×10^5 is shown in Table 2. The data were obtained by using image processing software and measuring along a line at a span-wise position of 187·5mm from mid-span (shown by a dashed line in Fig. 4).

https://doi.org/10.1017/S0001924000009544 Published online by Cambridge University Press

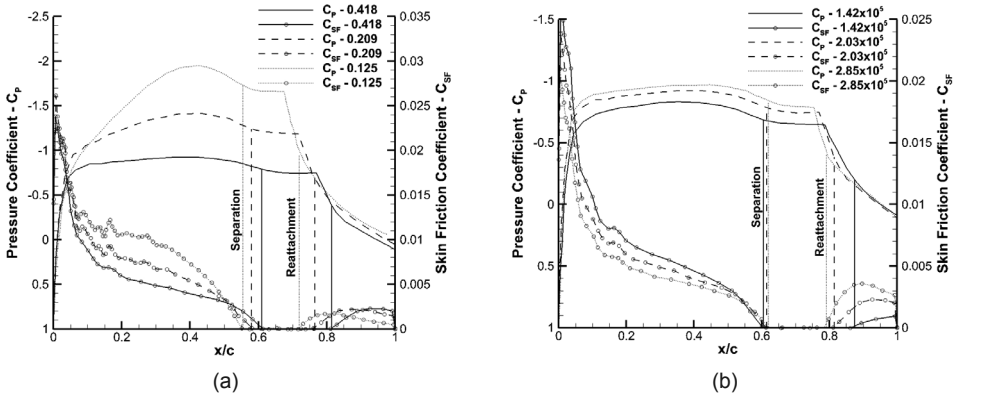


Figure 5. Suction surface pressure and skin friction at (a) varying ground clearance (Re = 2·03 × 10^5) and (b) varying Reynolds number (h/c = 0·418) for clean wing.

The results indicate that the separation point moves upstream and the bubble's length decreases as ground clearance is reduced. Increasing the Reynolds number also reduces the bubble length, but moves the separation point downstream. There is no indication in these flow visualisation images of a trailing-edge separation as described by Zerihan and Zhang[8].

3.3 Numerical simulation

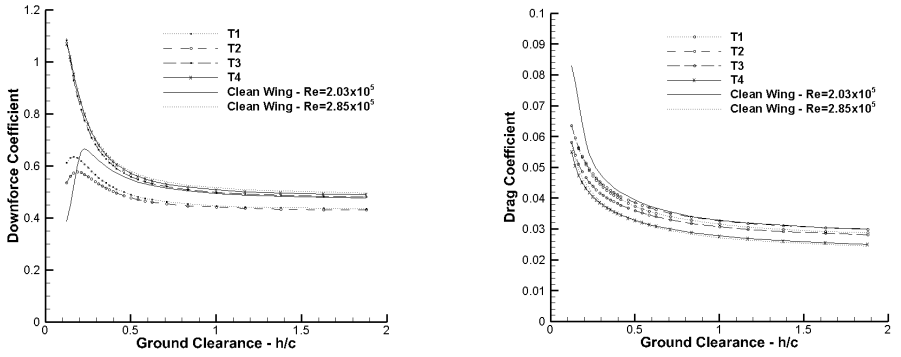
The surface pressures and skin friction coefficients on the aerofoil section at varying ground clearance and Reynolds number is shown in Figure 5(a). Similarly to the experimental results, as the wing moves closer to the ground the bubble's length reduces, with the separation and reattachment points both moving upstream. Clearly the larger adverse pressure gradient generated at lower ground clearances is causing the laminar boundary layer to separate earlier and then transition in the separated shear layer. The rate at which transition occurs is seemingly accelerated at lower ground clearance. Since the primary mechanism here is Kelvin-Helmholtz-type instabilities, which occur when there is velocity shear in the fluid, it can be concluded that the higher velocities developed at lower ground clearances, due to the constraining of flow between the wing and the ground, increases instability in the boundary layer.

Figure 5(b) shows that higher Reynolds number conditions cause transition to occur quicker in the separated shear layer; this combined with the later separation point results in a much shorter bubble. While there is little change in the separation point it is clear that the increase in energy due to the higher Reynolds number allows the boundary layer to remain attached slightly longer. In this case, a change in Reynolds number is equivalent to a change in flow velocity, as the chord length of the wing and fluidic properties of air remain unchanged. Therefore, the faster transition can be again attributed to greater velocity shear on the suction surface causing an increase in instability through a Kelvin-Helmholtz-type mechanism.

3.4 Transition Fixing

Due to wind-tunnel limitations it was not possible to test the current wing at higher Reynolds numbers. Hence it was not possible to reach a point, if it exists, where the forces are independent of Reynolds number, although, at the upper end of the tested range the difference between results is small. Fixed-transition tests were conducted in an attempt to replicate, at lower Reynolds numbers, the boundary-layer behaviour present on the wing at a higher Reynolds number.

https://doi.org/10.1017/S0001924000009544 Published online by Cambridge University Press



(a) (b)

Figure 6. (a) Downforce coefficient, C_F and (b) drag coefficient, C_D for different transition strips positioned at x/c = 0·25 at Re = 2·03 × 10^5 compared with clean wing results.

Force measurements were made on the transition-fixed configurations at three different Reynolds numbers: 1·42 ×10^5, 2·03 ×10^5 and 2·85 ×10^5. A total of four different transition strip configurations positioned at three different chord-wise locations were tested.

The force-measurement results (Fig. 6) show that only the T4 transition strip located at x/c = 0·25 led to results that could be considered similar to the clean wing at higher Reynolds numbers, showing good agreement on downforce and drag over the entire ground clearance range tested.

The force measurement results also show that there are differences in transition strip behaviour between the rough strips (T1 and T2) and the smooth strips (T3 and T4). Figure 6 shows the differences in strip behaviour at Re = 2·03 ×10^5. When comparing the different transitions strips with the clean wing, the rough strips produced a lower C_F, while the smooth strips showed similar results to the clean wing at a higher Reynolds number (2·85 ×10^5).

Surface flow visualisation (Fig. 7) shows the effect that each strip type had on the wing's lower surface boundary layer. While the T1 transition strip (rough) was capable of forcing the boundary-layer to transition and eliminate the separation bubble at the lowest Reynolds number,

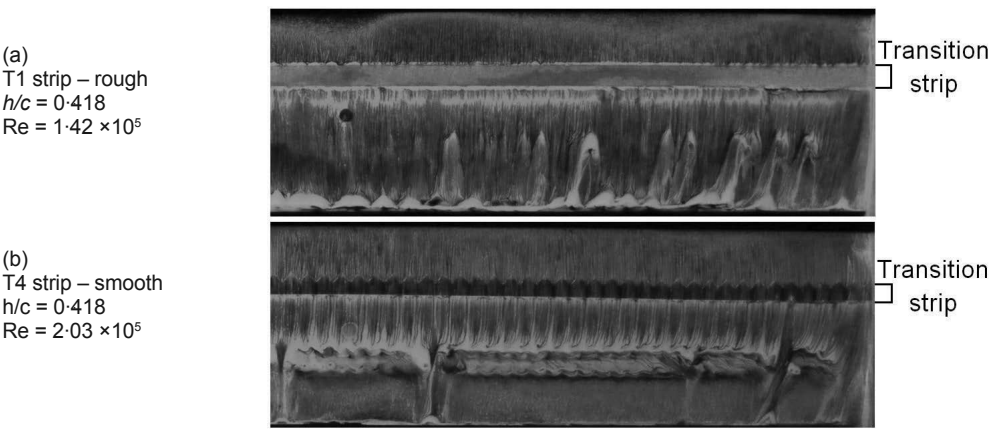


Figure 7. Semi-span flow visualisation results of different types of transition strips at different Reynolds numbers (leading edge uppermost, wing tip on the right).

https://doi.org/10.1017/S0001924000009544 Published online by Cambridge University Press

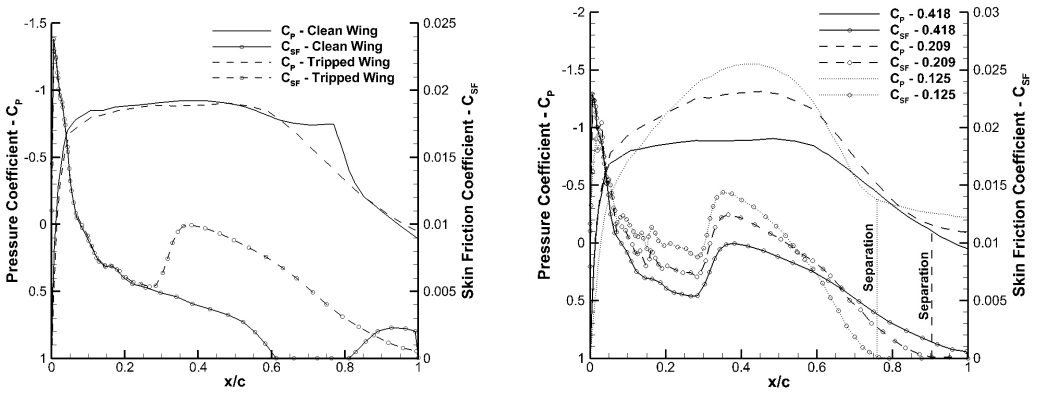


Figure 8. Suction surface pressure and skin friction at a) clean *vs* tripped wing (h/c = 0·418, Re = 2·03 ×10^5) and b) varying ground clearance (Re = 2·03 ×10^5) for tripped wing.

the T4 transition strip (smooth) was only capable of producing enough turbulence to affect the boundary layer such that its behaviour appears similar to a higher Reynolds number where the bubble is still present. The serrated leading edge of the T4 strip creates streamwise vortices, which appear similar to those defined in the natural transition model of White[22], which did not have enough energy to cause full transition to turbulence. However, the disturbances caused by the strip do accelerate the transition process, hence reducing the bubble length.

MSES allows boundary-layer trips to be simulated by forcing transition at a specified location (unless the e^N criterion has been met upstream and transition has already occurred). This method, however, is more representative of the rough strips for which transition occurs almost immediately rather than the smooth trips (T4).

The effect on the static pressure distribution and skin friction coefficient due to a boundary-layer trip placed at 0·25c on the aerofoil's suction surface is shown in Fig. 8(a). As observed in the experimental results (Fig. 6) the rough trip caused a reduction in both downforce and drag. The surface pressures show that the reduction in downforce is due to the elimination of the separation bubble. The presence of the bubble alters the effective geometry of the aerofoil and allows suction to be maintained. Although it cannot be seen in this two-dimensional analysis, the increase in suction on the lower wing surface will increase the lateral movement of air and thus increase force enhancement from the tip vortices.

It is clear from Fig. 8(b) that the larger suction levels, and accompanying adverse pressure gradient, associated with the reduced ground clearance are causing trailing-edge separation with the trip in place. As observed by Zerihan and Zhang[8], the separation point moves upstream as the wing moves closer to the ground. This indicates that the separation bubble, in addition to causing an increase in downforce by maintaining suction, also re-energises the boundary layer by effectively resetting it on reattachment and thus avoiding separation. Without the separation bubble present the turbulent boundary layer is not capable of overcoming the large deceleration of flow and separates closer to the trailing edge. This is because with the bubble present the majority of pressure recovery occurs soon after transition when turbulent mixing, which suppresses separation through momentum transfer normal to the wall, is at its highest.

https://doi.org/10.1017/S0001924000009544 Published online by Cambridge University Press

4.0 DISCUSSION

The force results showed similar trends to those previously published for an inverted wing in ground effect, both in terms of performance[9] and in terms of the influence that different Reynolds numbers have on the wing's performance[8].

The surface flow visualisation and numerical simulation showed the existence of a laminar separation bubble on the lower surface of the clean wing at all tested ground clearances and Reynolds numbers. Analysis of the separation bubble showed that both the length of the separation bubble and the onset of separation were dependent on the Reynolds number and ground clearance. Although the experimental force measurements showed a force enhancement and reduction region, the surface flow visualisation did not show a typical wing in ground effect trailing-edge separation, as described by Zerihan and Zhang[8] for higher Reynolds number values and lower ground clearance. Boundary-layer transition on the Tyrell 026 wing used by Zerihan and Zhang occurred through a short separation bubble at around 30% chord, which is close to the forced transition location (0·25(c)) used in this study for which separation was also observed. Therefore, the formation of a larger separation bubble, due to the lower Reynolds number and higher ground clearance compared to Zerihan and Zhang, combined with a geometry in which the adverse pressure gradient begins ~0·2*c* later, resulted in no trailing-edge separation occurring for the clean wing tests.

From the surface flow visualisation and force measurements it was noted that the rough and smooth transition strips behaved in distinct ways. Although the rough strips produced less downforce than the clean wing, they were capable of fixing transition and eliminating the separation bubble. On the other hand, the smooth transition strips produced a similar downforce to the clean wing at a higher Reynolds number, but were not capable of fixing the transition or eliminating the separation bubble.

The use of a rough transition strip and the effect it had on the laminar separation bubble highlighted the influence that the laminar separation bubble had on the wing's performance. On the clean wing more downforce was produced than on the wing with the transition strip at the same Reynolds number. This difference was shown to be due to an effective de-cambering of the wing when the separation bubble was eliminated.

As the Reynolds number was increased the separation bubble's influence on the wing's effective geometry reduced i.e. the rate of increase of downforce reduced as Reynolds number increased. Although there has been no measurement of the bubble's height in this study, Diwan[7] showed that as Reynolds number is increased the bubble's height decreased at a greater rate than its length. It can therefore be inferred, based on the results presented, that both reducing ground clearance and increasing Reynolds number causes a smaller and thinner bubble, thus limiting its effect on downforce generation.

As the wing's ground clearance is reduced the flow is constrained between the wing and the ground and accelerates, leading to an increase in downforce. Further reducing the ground clearance produces a reduction in bubble length, upstream movement of the separation point and a possible reduction in bubble height, which leads to a change in the effective wing shape similar to a reduction in wing camber. This explains the force reduction region shown in the force measurements.

5.0 CONCLUSION

The present work investigated the scale effect of an inverted wing in ground effect at –0·5° incidence. The initial experimental results showed the wing's performance was dependent on

https://doi.org/10.1017/S0001924000009544 Published online by Cambridge University Press

Reynolds number. Surface flow visualisation and numerical simulation showed the presence of a laminar separation bubble which was sensitive to Reynolds number and ground clearance. It was, therefore, postulated that both these parameters affected the growth of Kelvin-Helmholtz-type instabilities in the separated shear layer and altered the transition location. Different transition-fixing configurations were tested but only one (the vinyl strip with serrated leading edge) affected the boundary layer such that its behaviour was similar to a higher Reynolds number where the bubble is still present.

Two-dimensional numerical simulation showed that the formation of the bubble was dependent on the magnitude of the wing's adverse pressure gradient, Reynolds number and ground clearance. Hence, the results of this study are not limited solely to the GA(W)-1 aerofoil but are transferable to other low-Reynolds number wing-in-ground-effect cases.

The study highlights how boundary-layer behaviour affects the overall performance of the wing. Although the force-enhancement and -reduction mechanisms behind the performance of an inverted wing in ground effect are well documented, they do not fully explain the results obtained in this investigation; in particular, there is no evidence here of the trailing-edge separation, commonly thought to be the cause of the force reduction phenomenon. Instead, the separation bubble was shown to change the effective geometry of the wing and facilitated an increase in downforce. In comparison to the tripped wing, it was also found that the bubble re-energised the boundary layer to help it overcome the large adverse pressure gradients, which coincide with low ground clearances, and prevent trailing-edge separation.

This study was limited to the analysis of the laminar separation bubble's onset of separation and length, but further studies are required to understand how the bubble's height is affected by the Reynolds number and ground proximity, and the influence it has on the wing's performance.

ACKNOWLEDGEMENTS

The authors thank Professor Mark Drela for providing the MSES program for use in this report.

REFERENCES

1. MABEY, D.G. A review of scale effects in unsteady aerodynamics, *Prog Aerospace Sci*, 1991, **28**, pp 273-321.
2. BRASLOW, A. and KNOX, E. Simplified method for determination of critical height of distributed roughness particles for boundary-layer transition at Mach numbers from 0 to 5, Technical Note 4363, NACA, Langley Aeronautical Laboratory, 1958.
3. TANI, I. Low-speed flow involving bubble separations, *Progress in Aeronautical Sciences*, 1964, **5**, pp 70-103.
4. LIEBECK, R. and BLACKWELDER, R. Low Reynolds number – separation bubble, University of Southern California, Final Technical Report for contract N00014-84-K-0500 (Available from Defense Technical Information Center as AD-A199 378), 1987.
5. MUELLER, T.J. and BATILL, S.M. Experimental studies of separation on a two-dimensional airfoil at low Reynolds numbers, *AIAA J*, 1982, **20**, (4), pp 457-463.
6. GENC, M.S., KARASU, I. and ACIKEL, H.H. An experimental study on the aerodynamics of NACA2415 aerofoil at low Re numbers, *Experimental Thermal and Fluid Sciences*, 2012, **39**, pp 252-264.
7. DIWAN, S. and RAMESH, O.N. Laminar separation bubbles: dynamics and control, *Sadhana – Indian Academy of Sciences Proceedings in Engineering Sciences*, 2007, **32**, Part 1 and 2, pp 103-109.
8. ZERIHAN, J. and ZHANG, X. Aerodynamics of a single element wing in ground effect, 38th AIAA Aerospace Sciences Meeting and Exhibit, Reno, NV, USA. AIAA Paper 2000-0650, AIAA, 2000.
9. KNOWLES, K., DONOGHUE, D.T. and FINNIS, M.V. A study of wings in ground effect. Proc. RAeS Conference on Vehicle Aerodynamics, Loughborough, UK, 1994, pp 22.1–22.13.

https://doi.org/10.1017/S0001924000009544 Published online by Cambridge University Press

10. RANZENBACH, R. and BARLOW, J.B. Two-dimensional airfoil in ground effect, an experimental and computational study, Motorsports Engineering Conference and Exposition, Dearborn, MI, USA, SAE Paper 942509, 1994.
11. RANZENBACH, R. and BARLOW, J. B. Cambered airfoil in ground effect- wind tunnel and road conditions, AIAA 13th Applied Aerodynamics Conference, San Diego, CA, USA, AIAA Paper 95-1909, 1995.
12. RANZENBACH, R. and BARLOW, J. Cambered airfoil in ground effect – an experimental and computational study. In International Congress and Exposition, Vehicle Aerodynamics: Wind Tunnel, CFD, Aeroacoustics, and Ground Transportation Systems, Detroit, MI, USA, SAE Paper 960909, 1996.
13. JASINSKI, W. and SELIG, M. Experimental study of open-wheel race-car front wings, Motorsports Engineering Conference and Exposition, Dearborn, MI, USA, SAE Paper 983042, 1998.
14. ZERIHAN, J. and ZHANG, X. A single element wing in ground effect; comparisons of experiments and computation, In 39th AIAA Aerospace Sciences Meeting and Exhibit, Reno, NV, USA, AIAA Paper 2001-0423, 2001.
15. ZHANG, X., ZERIHAN, J., RUHRMANN, A. and DEVIESE, M. Tip vortices generated by a wing in ground effect, In 11th International Symposium on Applications of Laser Techniques to Fluid Mechanics, Lisbon, Portugal, IST, 2002.
16. MOLINA, J. and ZHANG, X. Aerodynamics of oscillating wings in ground effect, 48th AIAA Aerospace Sciences Meeting including the New Horizons Forum and Aerospace Exposition, Orlando, FL, USA. AIAA Paper 2010-318, 2010.
17. BEVES, C.C., BARBER, T.J. and LEONARDI, E. Airfoil flow separation suppression using dimples, The *Aeronaut J*, 2011, **115**, (1168), pp 335-344.
18. KNOWLES, K. and FINNIS, M.V. Development of a new open-jet wind tunnel and rolling road facility, in 2nd MIRA International Conference on Vehicle Aerodynamics, Coventry, UK, 20-21 October 1998.
19. VON DOENHOFF, A.E. and HORTON, E.A. A low-speed experimental investigation of the effect of a sandpaper type of roughness on boundary-layer transition, NACA Rep 1349, 1958.
20. VAN INGEN, J.L. A suggested semi-empirical method for the calculation of boundary layer transition region, Report Nos. V.T.H-71, Report V.T.H.-74 (in English), Delft, The Netherlands, 1956.
21. SMITH, A.M.O. and GAMBERONI, N. Transition, pressure gradient and stability theory, Proc. 9th Int. Congr. Appl. Mech, John Wiley and Sons, Chichester, UK, 1956.
22. WHITE, F.M. *Viscous Fluid Flow*, New York, USA, McGraw-Hill, 1974.

https://doi.org/10.1017/S0001924000009544 Published online by Cambridge University Press